

## Crystalline Block Copolymer Decorated, Hierarchically Ordered Polymer Nanofibers

**Xi Chen, Bin Dong, Bingbing Wang, Rucha Shah, and Christopher Y. Li\***

*Department of Materials Science and Engineering, Drexel University, Philadelphia, Pennsylvania 19104,  
United States*

*Received August 18, 2010; Revised Manuscript Received October 11, 2010*

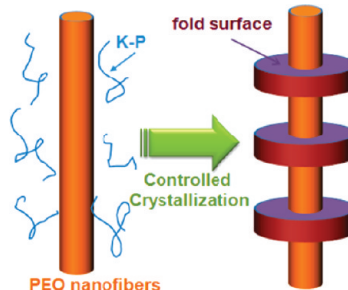
**ABSTRACT:** We report the formation of hierarchically ordered polymer nanofiber structures, named as nanofiber shish kebabs (NFSKs), by combining electrospinning and controlled polymer crystallization. Nanofibers were produced by electrospinning polycaprolactone (PCL), which was used as the shish, and a secondary polymer [either PCL or PCL-*b*-poly(ethylene oxide)] was decorated on the nanofiber by an incubation (slow crystallization) or a solvent evaporation (fast crystallization) method to form kabab lamellae. Selected area electron diffraction experiment showed that the PCL crystal *c* axis is parallel to the fiber axis in both shish and kebabs. The formation mechanism was attributed to soft epitaxy where crystallographic registration between the shish and the kebab was not needed. In block copolymer NFSKs, nanofiber-induced polymer crystallization brings the block copolymer to the vicinity of the nanofibers, and the block copolymer further phase separated into lamellar structure templated by the nanofiber. The resultant hierarchical architecture is of technological interest because it provides a platform for incorporating different functionalities into nanoscale polymer fibers in an ordered fashion.

### Introduction

Electrospinning is a useful method to produce continuous fibers with diameters ranging from micrometers to several tens of nanometers.<sup>1–5</sup> It can be applied to a wide range of polymers and inorganic materials.<sup>1–5</sup> Composite fibers with complex structures, such as core–shell, hollow, and necklace nanofibers, have been successfully fabricated.<sup>6–9</sup> Because of the diversity of this method, electrospinning has found applications in biomedical engineering,<sup>10–15</sup> catalysis,<sup>16</sup> filtration, and sensors.<sup>17–19</sup> With the development of numerous novel electrospinning techniques, such as bicomponent,<sup>20–22</sup> coaxial and two-flow/phase,<sup>23–26</sup> and layer-by-layer electrospinning,<sup>27</sup> great success has been achieved in controlling the surface morphology,<sup>28–32</sup> inner fiber phase separation,<sup>33,34</sup> and spatial alignment of nanofibers.<sup>35–38</sup> Recently, research in this field has been focused on introducing multicomponents into nanofibers to produce hybrid materials with hierarchical structures. The hierarchical structures can be achieved either during electrospinning or via a second deposition process. For example, introducing block copolymers into the systems leads to hierarchically ordered nanofibers.<sup>33,39–41</sup> Rutledge et al. have reported the formation of core–shell nanofibers by encapsulating block copolymer as the core component within a polymer shell and annealing these coaxial fibers above the glass transition temperature ( $T_g$ ) of the block copolymer.<sup>40</sup> Recently, Ji and Zhang fabricated porous carbon nanofibers by electrospinning a bicomponent polymer solution, followed by thermal treatment under various atmospheres. Because of relatively large surface area, the porous carbon nanofibers have found application as anode materials for rechargeable lithium ion batteries.<sup>42</sup>

The morphology of electrospun nanofibers can also be easily modified by introducing nanoparticles and/or polymers onto fiber surface. We recently reported that hierarchically ordered

**Scheme 1. Schematic Representation of Nanofiber Shish Kebabs Formed by PEO**



nanofibers can be fabricated by combining electrospinning and controlled polymer crystallization.<sup>43</sup> Poly(ethylene oxide) (PEO) single crystals were formed on the preformed PEO nanofibers as shown in Scheme 1. The unique nanoscale architecture, named as nanofiber shish kebab (NFSK),<sup>43</sup> resembles the conventional shish-kebab structure formed in polymers when they crystallize under an extensional field.<sup>44</sup> In NFSK, the preformed nanofibers served as the shish, and a secondary polymer was decorated on the nanofiber in the form of single-crystal lamellae. This architecture is of technological interest because it provides a platform for incorporating different functionalities into nanoscale polymer fibers in an ordered fashion. The orthogonal orientation of the lamellar crystals and the fiber axis also allows facile control over porosity and surface roughness for NFSK nonwoven sheets, which could be critical for biomedical applications. From both scientific and technological standpoints, it is of interest to control the shish and kebab structures. Previous work showed the feasibility of forming NFSK structures, and the shish- and kebab-forming polymers are the same (PEO). It would be beneficial if NFSK could be formed using other crystalline polymers and if these two structural units (shish and kebab) were composed of different polymers, because this can lead to better chemical and

\*Corresponding author: e-mail chrisli@drexel.edu; Tel 215-895-2083;  
Fax 215-895-6760.

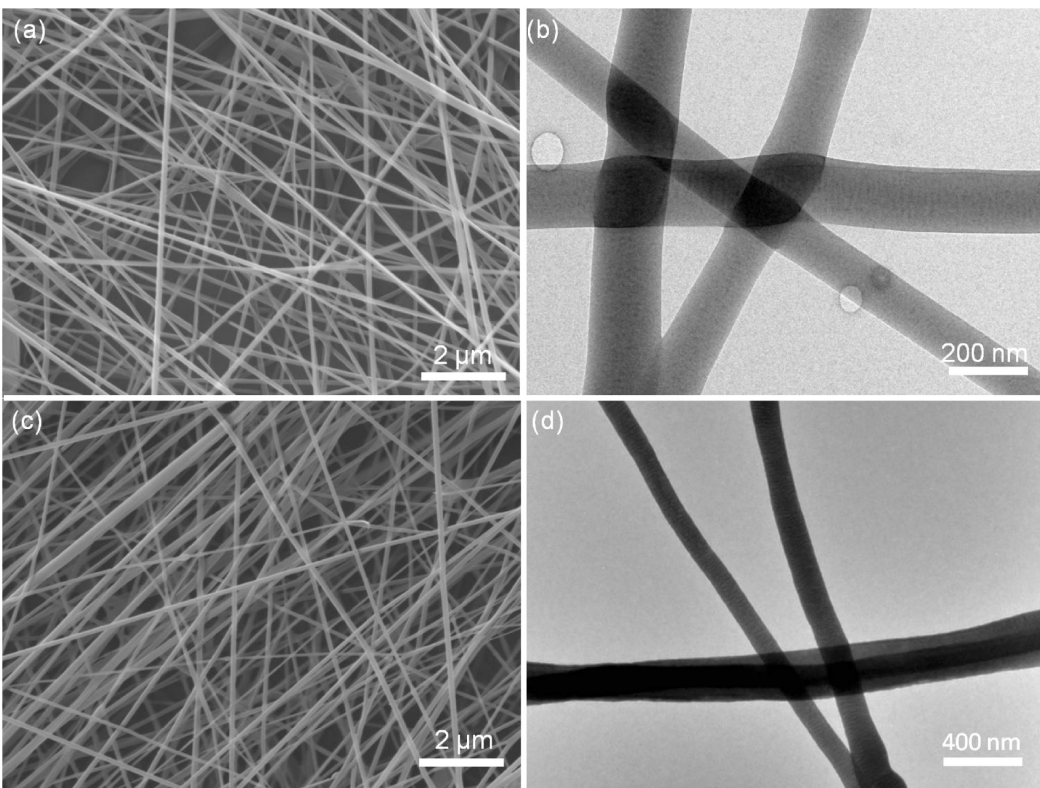


**Figure 1.** SEM (a, c) and TEM (b, d) images of electrospun nanofibers. (a, b) are PCL nanofibers and (c, d) are PEO nanofibers.

structural control of the nanofiber. In this paper, we report such NFSKs. In particular, polycaprolactone (PCL) was used to form nanofibers (hence the shish). In order to introduce a different polymer to form kebab crystals, polycaprolactone-*b*-PEO (PCL-*b*-PEO) was used. Uniform alternating patterns were formed on the nanofiber surface, and the detailed formation mechanism will be discussed.

## Experimental Section

**Materials.** PCL-*b*-PEO (5K–5K g/mol) and PCL (20K g/mol) were purchased from Polymer Source Inc. PCL (80K g/mol), poly(ethylene oxide) (PEO, 300K and 2K g/mol), trifluoroethanol (NMR grade, ≥99.5%), and *N,N'*-dimethylformamide (DMF, ACS reagent, ≥99.8%) were purchased from Aldrich. Ethyl acetate (ACS grade, ≥99.5%) was purchased from VWR. All materials were used as received.

**Electrospinning of Nanofibers.** PCL nanofibers were electrospun from 10 wt % PCL (80K g/mol) trifluoroethanol solution. The feeding rate, voltage, and collecting distance were controlled to be 0.3 mL/h, 18 kV, and 15 cm, respectively. PEO nanofibers were electrospun from 9 wt % PEO (300 K g/mol) DMF solution, which was formed by dissolving PEO at 65 °C under continuous stirring for 1 h. The feeding rate, voltage, and collecting distance for electrospinning were controlled to be 0.5 mL/h, 18 kV, and 13 cm. A piece of aluminum foil was used as the ground collector. Carbon-coated nickel TEM grids were used to directly collect nanofibers for the TEM experiment. Glass slides were also used to collect nanofibers for SEM observation.

**Polymer Crystallization on Nanofibers.** *1. Crystallization by Solution Incubation.* Either ethyl acetate or DMF was used to prepare PCL-*b*-PEO solution at ~60 °C. PCL nanofibers and PEO nanofibers were incubated in PCL-*b*-PEO/ethyl acetate and PCL-*b*-PEO/DMF solutions of various concentrations with a range of incubation times, respectively. After incubation, the nanofibers were then taken out from the solution and washed three times with the corresponding solvent to remove free polymers. The nanofibers were then dried under the vacuum overnight.

*2. Crystallization by Solvent Evaporation.* The nanofibers were collected on the surface of TEM grids. Approximately 2 μL of PCL-*b*-PEO/ethyl acetate and PCL-*b*-PEO/DMF solutions were drop-casted on PCL nanofibers and PEO nanofibers, respectively. The nanofibers were then dried at room temperature. Solvent evaporation on PCL nanofibers was performed under saturated ethyl acetate vapor, allowing sufficient time for crystallization before all the ethyl acetate evaporated. Compared with crystallization by solution incubation, crystallization by solvent evaporation in the present work was controlled to take place within a relatively short time (2–10 min).

**Characterization.** Environmental scanning electron microscopy (ESEM, FEI XL30) and transmission electron microscopy (TEM, JEOL 2100JEM) were used to characterize nanofiber morphology and structure before and after surface modification. The SEM samples were prepared by depositing electrospun nanofibers onto the surface of glass slides followed by controlled polymer crystallization. To increase conductivity, samples were coated with platinum (25 s, 40 mA) by a Gressington sputter coater 208HR before SEM observation. All SEM samples were imaged at an acceleration voltage of 10 kV. The TEM samples were prepared by collecting electrospun nanofibers onto a carbon-coated nickel TEM grid. In order to increase contrast, ruthenium tetroxide ( $\text{RuO}_4$ ) was used to stain some of the TEM samples as detailed in the Discussion section. An acceleration voltage of 120 kV was used for TEM experiments. The diameters of nanofibers and the densities of shish kebabs along nanofibers were calculated on the basis of SEM images using ImageJ software.

## Results and Discussion

**Electrospinning of Nanofibers.** PCL nanofibers were obtained by electrospinning 10 wt % PCL/trifluoroethanol solution as discussed in the Experimental Section. Figure 1a,b shows SEM and TEM images of the resultant PCL nanofibers. The average diameter of PCL nanofibers is ~200 nm. PEO nanofibers were obtained by electrospinning 9 wt % PEO/DMF

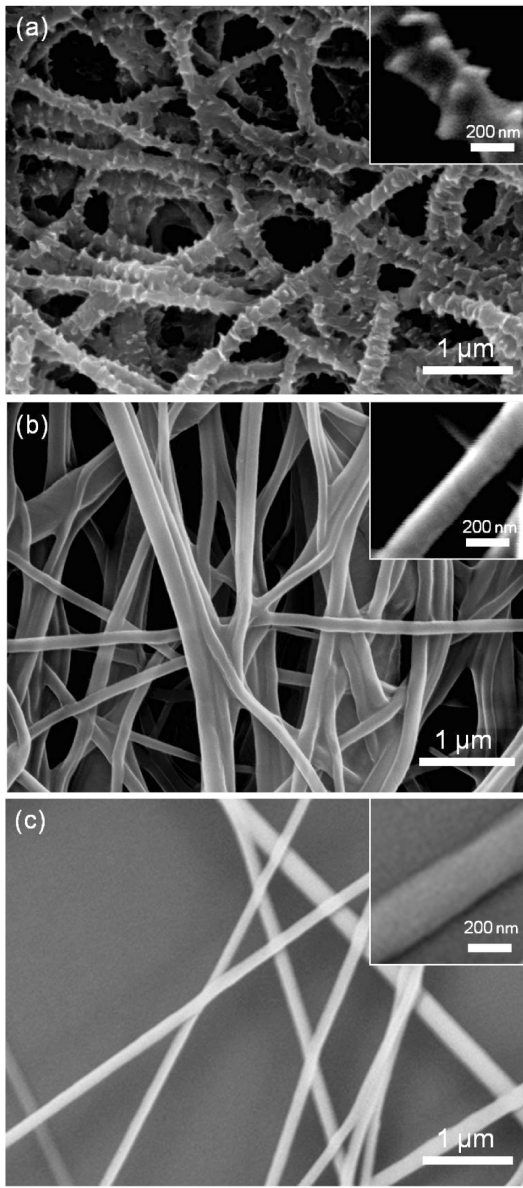


**Figure 2.** SEM images of PCL nanofibers after incubating in (a) DMF, (b) ethyl acetate, and (c) pentyl acetate for 1 h.

solution as stated in Experimental Section. Figures 1c,d show SEM and TEM images of the PEO nanofibers. The average fiber diameter is  $\sim 270$  nm. These nanofibers will then be used as one-dimensional templates for NFSK formation detailed as follows.

**Homopolymer Crystallization on Nanofibers. Forming NFSK<sup>PCL/PCL</sup> Using Solvent Evaporation.** In our previous study, NFSKs were formed using controlled crystallization, and PEO was used as the model polymer; the central shish was PEO nanofiber, and the kebabs were PEO lamellar crystals.<sup>43</sup> Herein we use NFSK<sup>PEO/PEO</sup> to describe this structure with the first and second PEO in the superscript denoting the shish- and kebab-forming polymers, respectively. DMF was used as the solvent in PEO crystallization process. To form NFSK structure on PCL nanofibers, in the present work, DMF was first selected as the solvent. Pure DMF was used for incubating PCL nanofibers as a control experiment. The fiber was incubated in DMF for 1 h and was rinsed with the same solvent three times. The fiber/DMF suspension was then spin-coated at  $\sim 1500$  rpm to remove most of the solvent. Figure 2a shows the resultant structure.

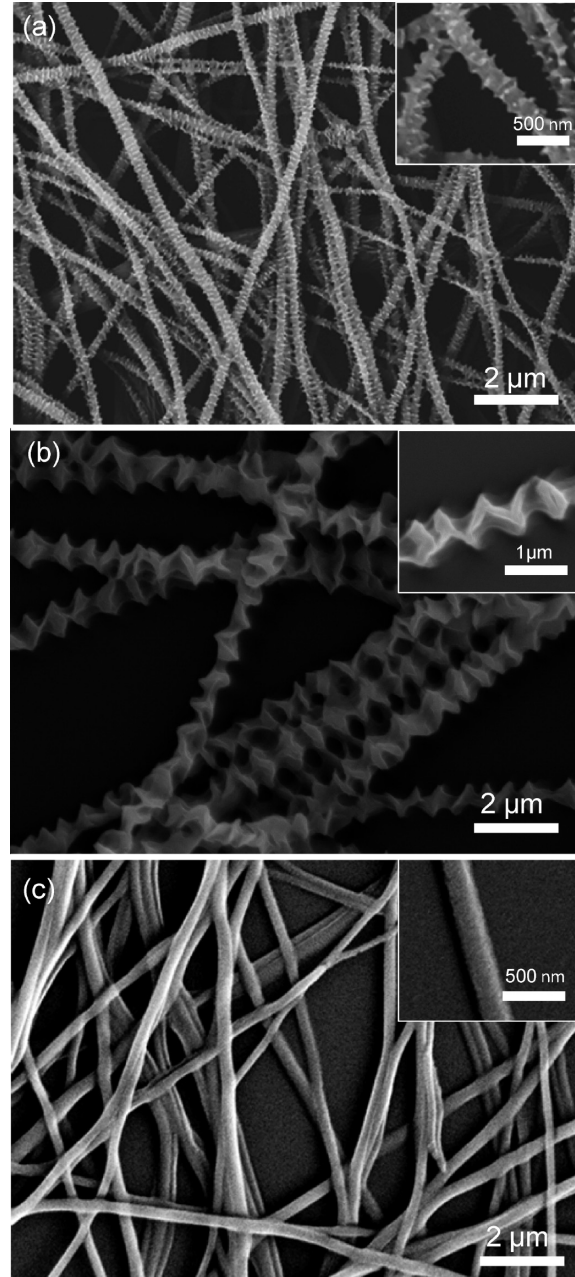


**Figure 3.** SEM images of PCL nanofibers solvent casted with (a) 1% PCL/ethyl acetate solution, (b) 1% PCL/pentyl acetate, and (c) PCL nanofibers solvent casted with a 0.1% PEO (2K g/mol)/ethyl acetate solution.

Small crystallites can be clearly seen, suggesting that NFSKs were formed. Of interest is that incubating PCL nanofibers in pure DMF solvent led to the formation of NFSKs. The NFSK<sup>PCL/PCL</sup> structure in Figure 2a is remarkably similar to that of the NFSK<sup>PEO/PEO</sup> previously reported: The fiber surface is coated with a layer of edge-on crystals, which are located along the fiber axis. The PCL crystal normal is relatively parallel to the nanofiber axis. Since pure DMF was used for incubation, the formation of NFSK<sup>PCL/PCL</sup> has to be caused by the crystallization of PCL that was dissolved from the fiber surface during incubation. Therefore, while incubating PCL nanofibers in pure DMF provides a facile method to fabricate NFSK<sup>PCL/PCL</sup>, it is not a good candidate for conducting quantitative study on PCL nanofiber-induced solution crystallization as obtaining the concentration of the PCL solution on the fiber surface is difficult. To avoid the solvent effect, pentyl acetate and ethyl acetate were

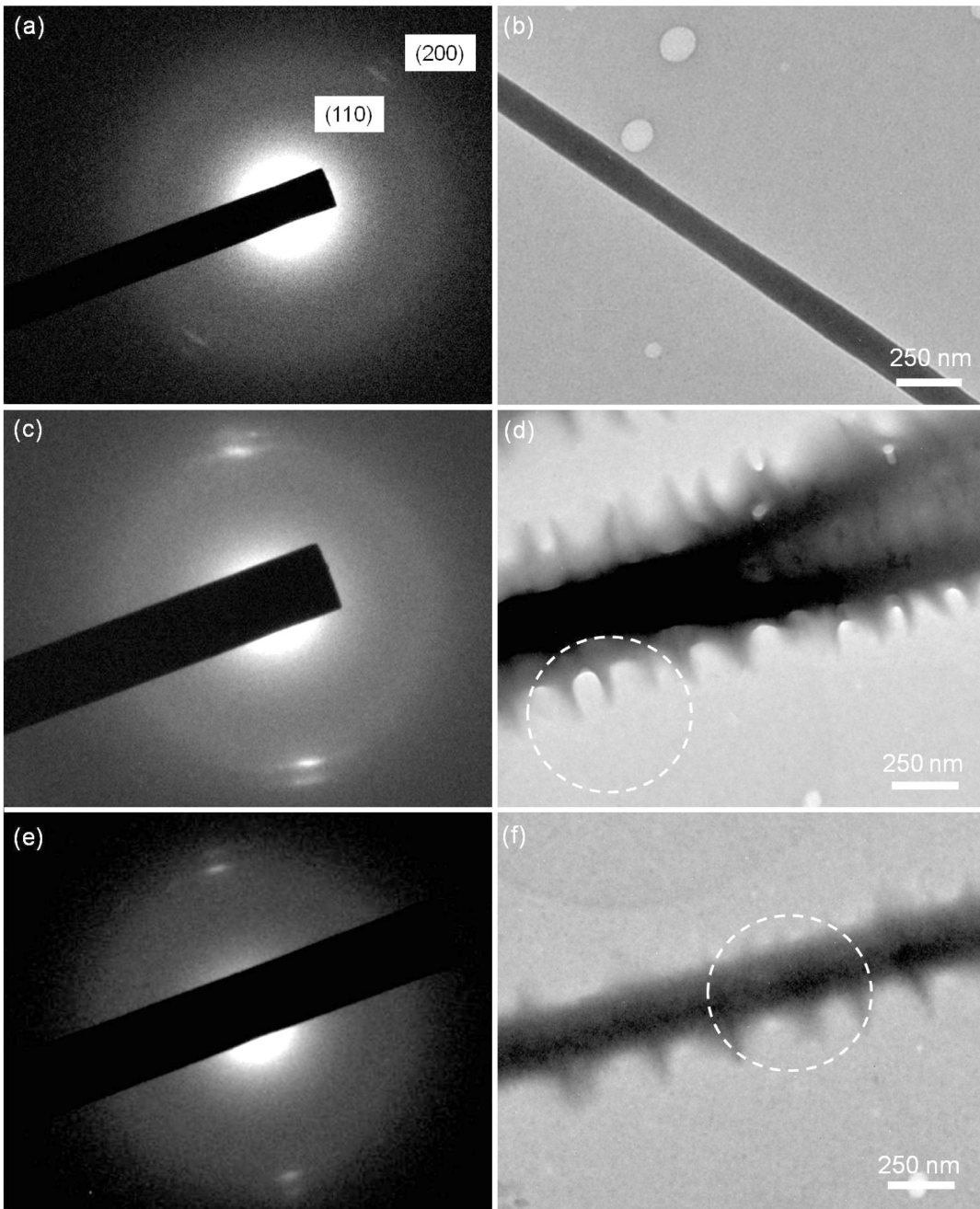


**Figure 4.** Electron diffraction pattern and bright field TEM image of a PCL nanofiber (a, b), PCL homopolymer kebabs (c, d), and PCL nanofibers with PCL homopolymer shish kebabs (e, f). The circles in (d) and (f) indicate the selected areas.

selected because they are nonsolvents of PCL at room temperature while they can readily dissolve the latter at  $\sim 60^\circ\text{C}$  and the solutions can remain stable for several hours. Figure 2b,c clearly shows that after incubating in pure ethyl acetate and pentyl acetate for 1 h at room temperature the PCL nanofiber surface was still smooth, and no shish-kebab structure was observed.

After confirming that both ethyl acetate and pentyl acetate are unable to dissolve PCL nanofiber during the incubation process, both solvents were used to form the kebab-forming solution with a concentration of 1% PCL (20K g/mol). 2  $\mu\text{L}$  of the solution was cast on the surface of PCL nanofibers. During this process, PCL concentration along nanofibers increases rapidly and PCL crystallizes on the surface of nanofibers. Hence, it is referred to as the solvent evaporation method to form NFSKs. Figures 3a,b show the SEM images

of the resulting structure. It is evident that NFSKs<sup>PCL/PCL</sup> were formed. In Figure 3a, the kebab crystals are uniformly spread along the entire nanofibers without completely wrapping around the nanofibers, and the overall morphology is similar to that of Figure 2a. However, in Figure 3b, the kebab crystals completely wrap around the nanofiber and form toroid crystals, similar to those observed in NFSK<sup>PEO/PEO</sup>.<sup>43</sup> This difference could result from the competition between nucleation, crystal growth, and the solvent evaporation, which will be discussed later in the paper.

To better demonstrate the orientation of polymer chains in nanofibers and kebabs, selective area electron diffraction (SAED) was employed.<sup>43,45</sup> Figure 4a shows SAED pattern from a PCL nanofiber, and Figure 4b shows the corresponding PCL nanofiber with the right orientation. Two pairs of reflection arcs were observed, and they can be ascribed to

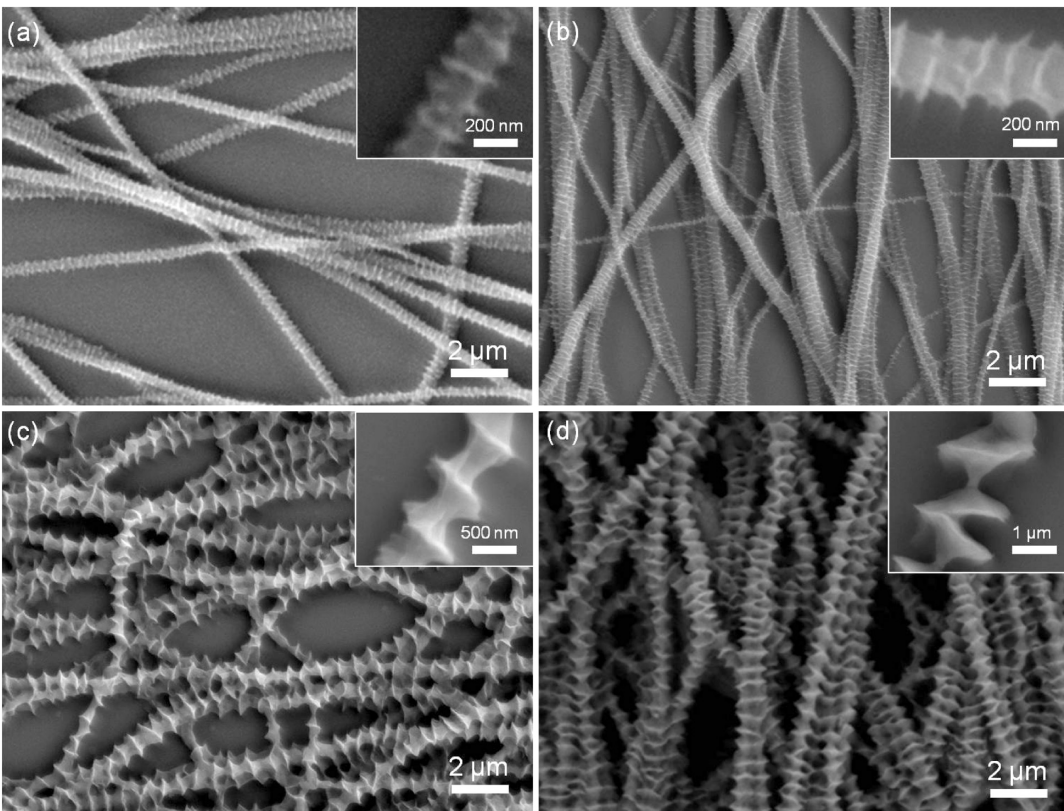


**Figure 5.** PCL nanofibers incubated in 1% PCL/pentyl acetate for (a) 5, (b) 15, (c) 30, and (d) 60 min.

(110) and (200) planes following the orthorhombic unit cell of PCL with  $a = 0.748$  nm,  $b = 0.498$  nm, and  $c = 1.726$  nm. Both (110) and (200) planes are parallel to the fiber axis, indicating the PCL chain axis is also parallel to the fiber axis. Diffraction patterns from PCL homopolymer kebabs and NFSK<sub>PCL/PCL</sub> were also obtained as shown in Figures 4c,e while Figures 4d,f are the corresponding morphologies with the circles denoting the selected areas. Both Figures 4c and 4e are similar to that the SAED pattern from the neat nanofiber (Figure 4a). We can then conclude that the crystal  $c$  axis in both shish and kebabs are parallel to the fiber axis.

The formation mechanism of NFSK<sub>PCL/PCL</sub> is similar to that of NFSK<sub>PEO/PEO</sub>, which follows soft epitaxy-governed crystal growth. During electrospinning, PCL polymer chains are stretched and aligned parallel to the fiber axis as shown in Figures 4a,b. When free PCL chains from the solution nucleate on the nanofiber surface, the chain tends to orient parallel to the fiber axis although a strict crystallography matching between the nanofiber and the kebabs may not be fulfilled. It is similar to the classic polymer shish-kebab structures: because polymer chains have a uniaxial fiber orientation in the shish, while the kebabs are single-crystal lamellae, crystallographic lattice matching between the shish and the kebab can, in the best scenario, only be fulfilled at a few locations at the shish/kebabs interface. Hence, the overall relationship between the shish and the kebab is best described as soft epitaxy. Note that the mechanism is similar to controlled crystallization on carbon nanotubes (CNTs) surface.<sup>46–52</sup> Size-dependent soft epitaxy was observed in the polyethylene (PE)/NHSK case; i.e., when the diameters of CNTs are small (less than 20 nm), PE chains in the kebabs are parallel to the CNT axis, while when the diameters of the CNTs are large ( $> 150$  nm), molecular epitaxy, with crystallographic matching between the graphene lattice and the polymer chain, dominates the crystal growth and multiorientation of the

crystal lamellar was observed. In the present case, although the nanofiber diameter is relatively large, we still observed soft epitaxy because all the chains in the nanofibers were aligned parallel to the fiber surface evidenced by the SAED experiment, while in the CNT case, graphene lattices have different orientations for CNTs with different chiralities.

Although strict crystallographic matching is not required in soft epitaxy, the compatibility of the two materials is important because the kebab materials need to be adsorbed onto the fiber surface prior to the crystallization process. As a control experiment, 0.1 wt % PEO (2K g/mol)/ethyl acetate solution was solvent-casted on the surface of PCL nanofibers under the same experimental condition (Figure 3b). NFSK morphology was not observed. This was attributed to the limited energy gain for PEO to crystallize onto the PCL surface. In such case, homogeneous nucleation of PEO is a more favorable process and NFSK of PEO kebabs on PCL were not formed.

*Forming NFSK<sub>PCL/PCL</sub> Using Solvent Incubation.* In solvent evaporation, the kebab crystals formed with 1% PCL/ethyl acetate did not completely wrap around the PCL shish (Figure 3a). This could be due to the competition between the growth of the kebab crystals and the heterogeneous nucleation of new kebabs in a short time frame. Given enough time and concentration gradient, toroid crystals have been formed in NFSK<sub>PCL/PCL</sub> formed via solvent evaporation 1% PCL/pentyl acetate (Figure 3b). It is of interest to capture the formation process of toroid crystals.

To this end, we used solution incubation method to fabricate NFSK<sub>PCL/PCL</sub>. PCL nanofibers were immersed in 1% PCL/pentyl acetate, and the formation of toroid kebabs was studied in time sequence. After 5 min incubation, kebab crystals were formed along the nanofibers (Figure 5a). The morphology is similar to Figures 2a and 3a with small crystallites decorating on the nanofibers. Given longer time

(15 min), those crystals were able to completely wrap around the shish (Figure 5b) with an average period of 140 nm between adjacent kebabs. The toroid kebabs started to collapse after extended incubation time. For example, after 30 min incubation, the kebab period increased to ~640 nm due to the collapse/merge of adjacent kebabs. In some places, the size of nanofibers also increased to ~400 nm, probably due to the coating of distorted toroid crystals (Figure 5c). After 60 min of the incubation, the kebab period further increased to ~1  $\mu$ m as shown in Figure 5d.

This series of experiments revealed that the formation of NFSK<sup>PCL/PCL</sup> started with uniformly distributed crystallites with the lamellar normal approximately parallel to the fiber axis. These crystallites further evolved into toroid crystals wrapping the nanofiber. As the toroids grew larger, adjacent lamellae merged, either during the growth or during the sample preparation process. In the ethyl acetate system, the crystal growth rate was much less compared with that in the pentyl acetate system under our experimental conditions; therefore, small crystallites were observed in the former system while large toroids were observed in the latter in both solvent evaporation and incubation experiments.

**PCL-*b*-PEO Crystallization on PCL Nanofibers.** *Forming NFSK<sup>PCL/PCL-*b*-PEO</sup> Using Solvent Evaporation.* Of great interest is to pattern block copolymers on nanofiber surface because curved convex surface could affect block copolymer phase separation.<sup>48,53,54</sup> Furthermore, hierarchical nanofibers with alternating patterns on the surface can be fabricated, and it can also provide another means to control the tomography of nanofiber surface for various applications. In the present study, both solvent evaporation and incubation methods were used to crystallize PCL-*b*-PEO onto PCL nanofibers. Ethyl acetate was used as the solvent for the crystallization of PCL-*b*-PEO on PCL nanofibers because of the poor solubility of PEO in pentyl acetate. In the solvent evaporation process, similar to previously discussed, a fixed amount of polymer solution was drop-casted on the nanofiber surface, and as the solvent evaporated, the solution concentration increased and the polymer crystallized on the nanofiber surface. Figure 6 shows the morphology of NFSK<sup>PCL/PCL-*b*-PEO</sup> formed by PCL nanofiber-induced PCL-*b*-PEO crystallization. Different from previous homopolymer system, “centipede-like” structure was formed in the PCL-*b*-PEO case with nanofibers forming the body of the centipedes and PCL-*b*-PEO crystals forming the feet (Figures 6a–c). The distinct feature is that the kebab crystals appeared to be confined near the substrate; they grew along the direction which is perpendicular to the fiber axis, leading to the formation of 2D NFSK<sup>PCL/PCL-*b*-PEO</sup>. This unique morphology can be attributed to the enrichment of block copolymers at the interface of nanofibers and substrate before stable nuclei could be formed on top of the nanofiber during the solvent evaporation process. The morphology resembles the 2D NHSKs formed on CNTs using a physical vapor deposition (PVD) method in which case oligomers of PE and nylon-6,6 were formed during PVD, and they subsequently deposit/crystallize on CNTs with the long axis of rodlike polymer crystals being perpendicular to the CNT axis.<sup>49,50</sup>

Block copolymer structure cannot be clearly revealed from the SEM image (Figure 6). To this end, TEM experiments were conducted, and Figure 7a shows a representative image of NFSK<sup>PCL/PCL-*b*-PEO</sup>. Note that the sample was stained with RuO<sub>4</sub>, and in Figure 7a, the dark stripes are PCL segments and the light lines are PEO segments. It is evident from the image that block copolymer phase-separated into lamellar structure along the nanofiber and the lamellar normal is parallel

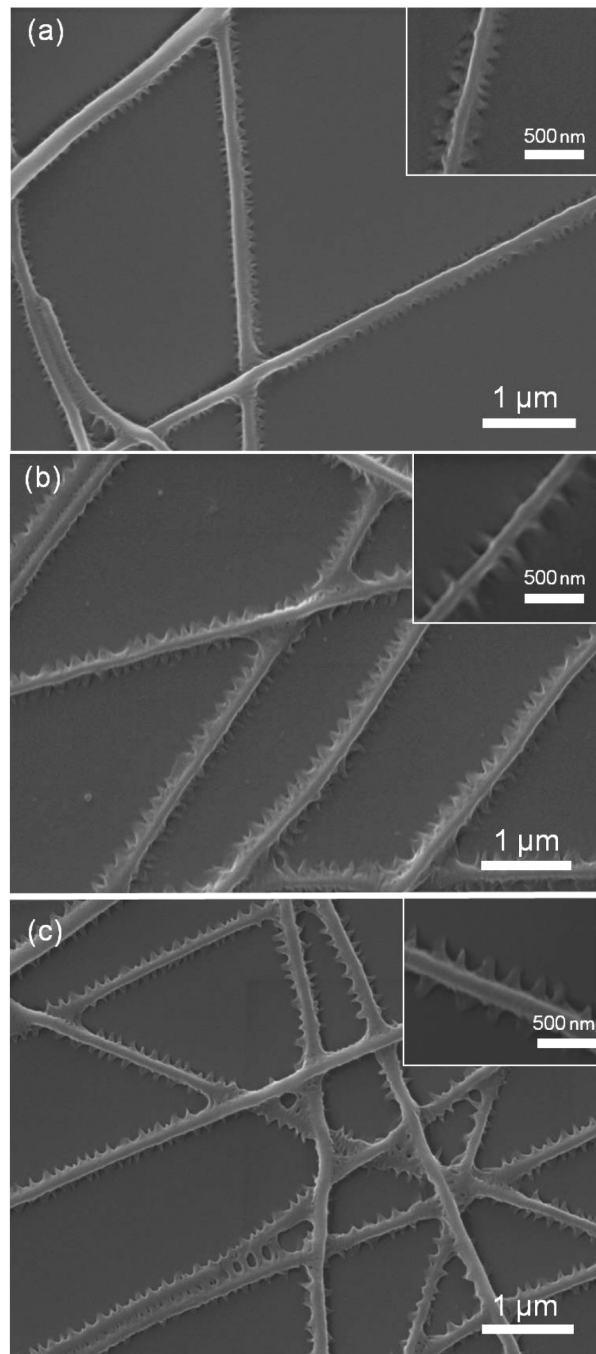


**Figure 6.** Solvent-cast PCL-*b*-PEO of different concentrations on PCL nanofibers: (a) SEM image of 0.00075% PCL-*b*-PEO; (b) SEM image of 0.0075% PCL-*b*-PEO; (c) SEM image of 0.075% PCL-*b*-PEO.

with the fiber axis. While SEM shows that the areas between adjacent kebabs are free of PCL-*b*-PEO, the TEM image suggests that the block copolymer covers the entire fiber surface. PCL-*b*-PEO stripes form patches with different sizes, and the average distance between adjacent patches is ~170 nm, corresponding to the period of the kebabs observed in the SEM image. Since our earlier control experiments showed that PEO was unable to form oriented lamellar crystals on the PCL fiber surface, the formation of NFSK<sup>PCL/PCL-*b*-PEO</sup> must be driven by nanofiber-induced PCL crystallization as shown in Scheme 2. PCL segments in the block copolymer tend to crystallize on the PCL nanofiber surface due to the favorite heterogeneous nucleation process. Once the PCL segments nucleated on the nanofiber surface, PEO segments are excluded

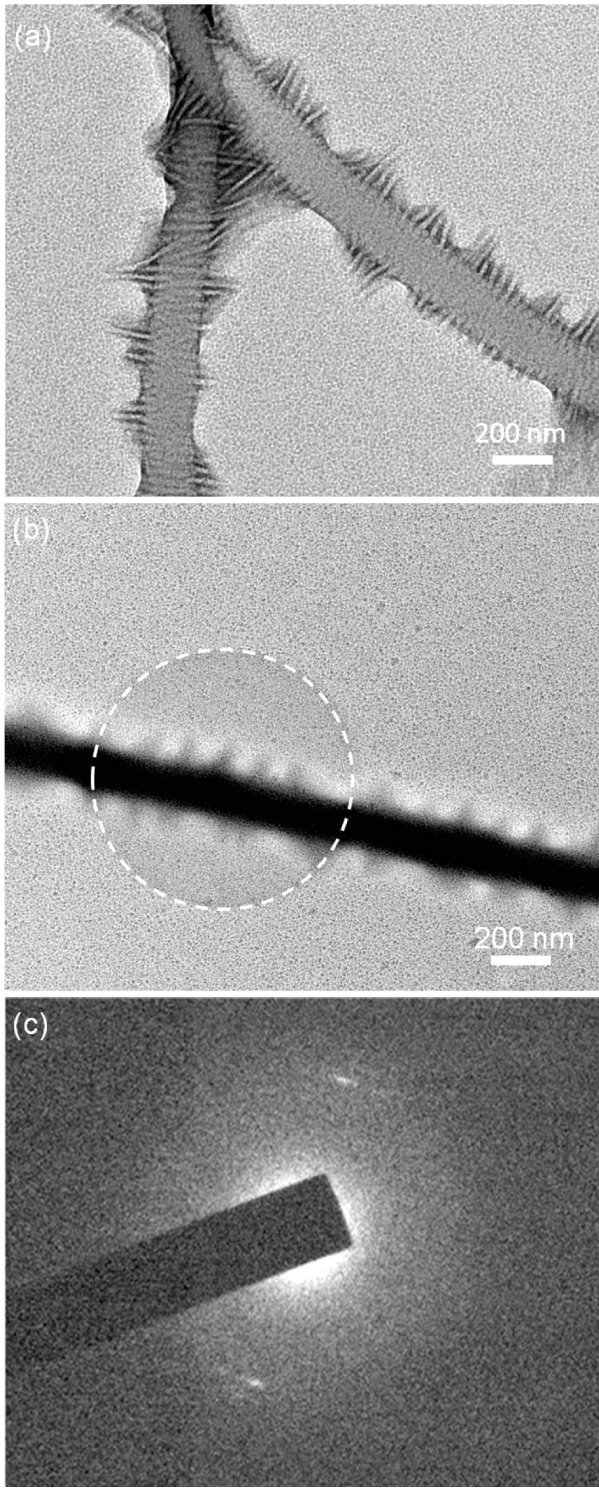
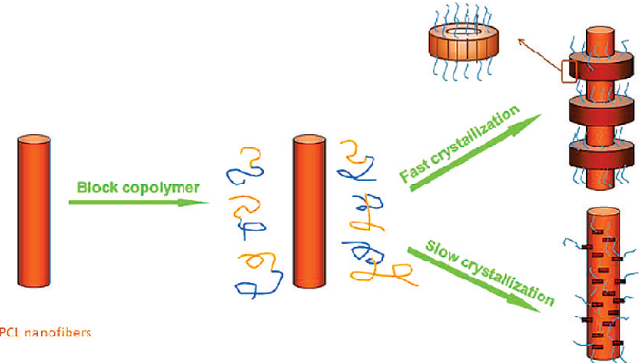


**Figure 7.** TEM stained image (a), unstained image (b), and the corresponding electron diffraction pattern (c) of PCL nanofiber with PCL-*b*-PEO block copolymer via solvent evaporation using 2  $\mu$ L 0.075% PCL-*b*-PEO/ethyl acetate.

from the PCL crystal. The previously discussed soft epitaxy mechanism of nanofiber-induced crystallization directly leads to the orthogonal orientation of the block copolymer lamellae and the fiber axis, as clearly revealed in Figure 7a. Figures 7b,c show the TEM image of a NFSK<sup>PCL/PCL-*b*-PEO</sup> and the corresponding SAED pattern with the correct orientation. Both (110) and (200) diffractions are seen and the orientation also suggests that chains in both block copolymer and nanofibers are parallel to

**Scheme 2. Schematic Representation of the Formation of Block Copolymer Nanofiber Shish Kebab**



the fiber axis. Only diffractions from PCL crystal are observed in Figure 7c, which indicates that diffractions from PEO were too weak to record in our experimental condition.

The concentration dependence of the kebab periods and diameters was statistically studied based on 200 nanofibers, and Figure 8 shows the histograms of the periods of NFSK and the size of kebab crystals. The kebab periods increased from  $\sim$ 110 to  $\sim$ 160 nm as the solution concentration increased from 0.00075 to 0.0075 wt %. Further increase of the concentration to 0.075 wt % did not change the period significantly. The average period for the 0.075 wt % sample was  $\sim$ 170 nm. Similar to the CNT NNSK case, the period of NFSK is determined by the concentration gradient along the nanofiber during the kebab crystallization process and normally decreases with increasing the solution concentration. The increase of distance from 110 to 170 nm when the concentration increases from 0.00075 to 0.075 wt % could be explained by the merging (collapse) of adjacent kebab crystals as a result of the capillary force between adjacent kebabs (Figure 7a).<sup>43</sup> The kebab size is also concentration dependent: as the concentration increases from 0.00075 to 0.075 wt %, the average kebab size increases from 118 to 162 nm. Further increase of concentration did not result in further increase in kebab size.

*Forming NFSK<sup>PCL/PCL-*b*-PEO</sup> Using Solvent Incubation.* Incubation was also used to perform slow crystallization of block copolymer on PCL nanofibers. Comparing with solvent evaporation, incubation has a better control over the experimental conditions. Crystallization time and solution concentration were varied to study the crystallization process. 15 wt % PCL-*b*-PEO solution in ethyl acetate was first used as the incubation solution. Considering the low vapor pressure of ethyl acetate, incubation was performed in saturated ethyl acetate vapor environment. Figures 9a–c show NFSK<sup>PCL/PCL-*b*-PEO</sup> after 40, 50, and 60 min incubation. It is clear that the formation of NFSK starts from the formation of randomly distributed nuclei. As the incubation time increased, the density of nuclei on nanofibers increased from an average of  $2.5 \times 10^4 \text{ nm}^2$  (Figure 9a) to  $3.3 \times 10^4 \text{ nm}^2$  (Figure 9c). The size of the crystals increased from  $43 \pm 11 \text{ nm}$  (Figure 9a) to  $70 \pm 13 \text{ nm}$  (Figure 9c). All the measurements are based on a statistical study of 200 data points. Figure 9d shows a TEM image of NFSK<sup>PCL/PCL-*b*-PEO</sup>, and similar to the previous, block copolymer phase separates on the nanofiber surface and the lamellar normal is parallel to the fiber axis. Note that the SEM samples were coated with platinum; therefore, the kebabs in TEM image appear to be smaller than those in SEM image.

Concentration is another important parameter in the solution crystallization process. Figures 10a–c show NFSK<sup>PCL/PCL-*b*-PEO</sup> after 10 min incubation in 15, 18, and

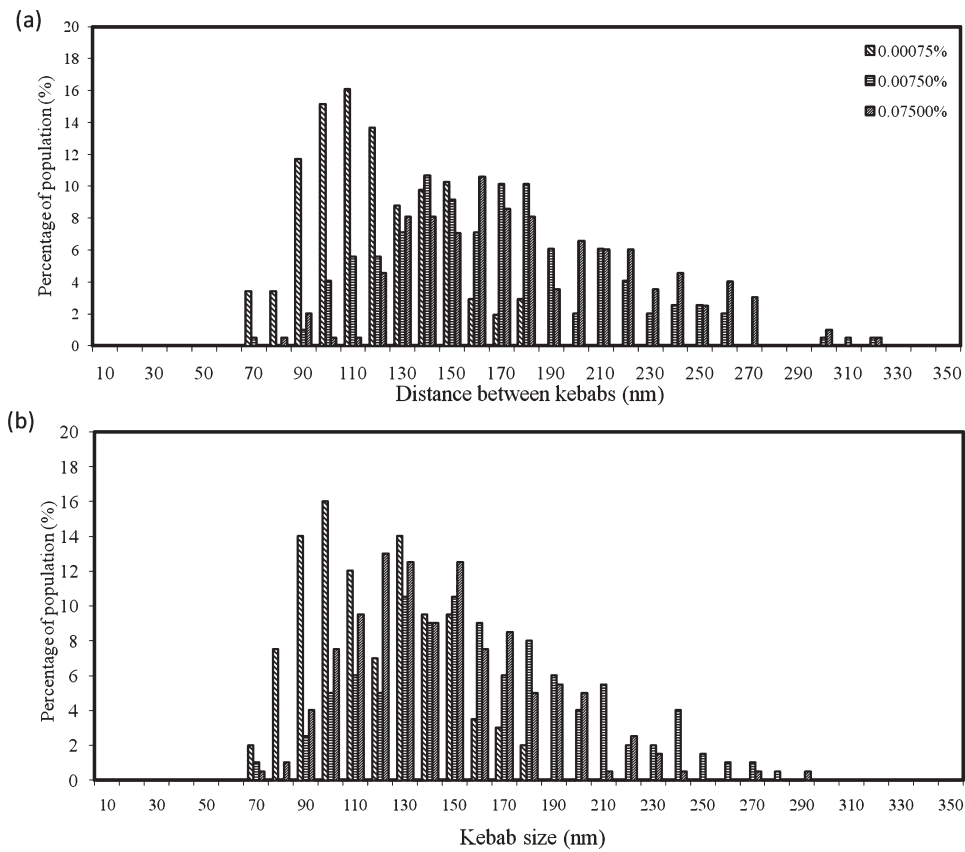


**Figure 8.** Histograms of (a) kebab period and (b) kebab size.

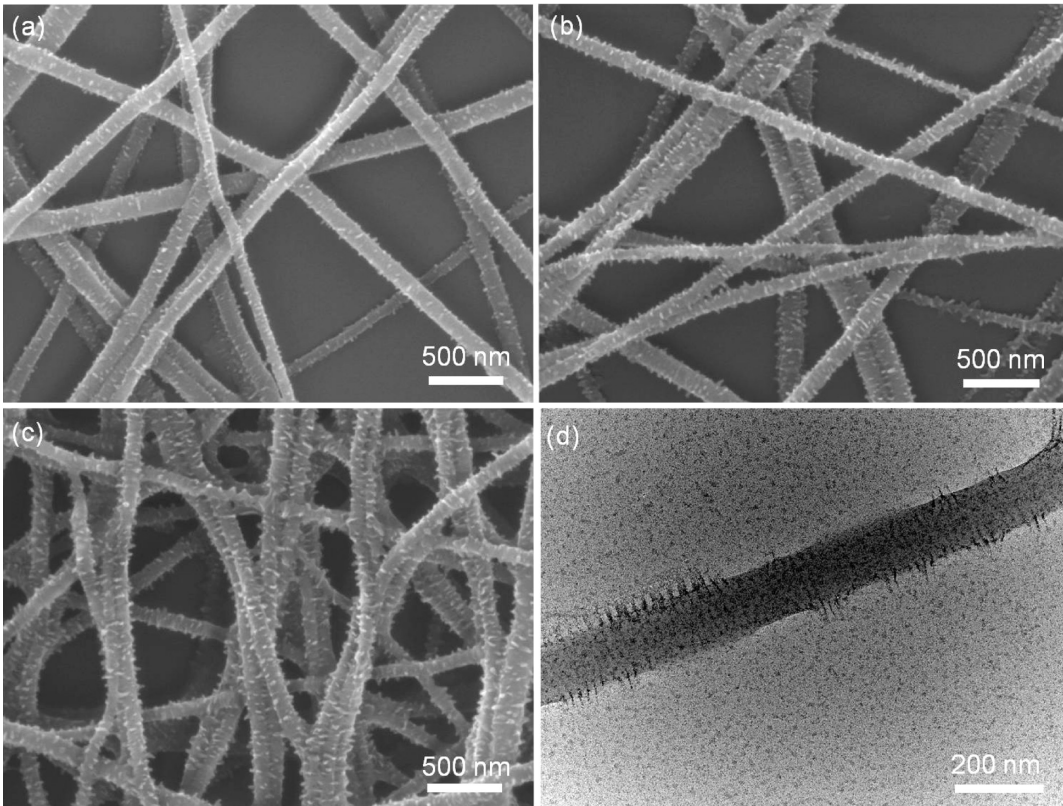


**Figure 9.** SEM images of PCL nanofibers incubated in 15% PCL-*b*-PEO/ethyl acetate for (a) 40, (b) 50, and (c) 60 min. (d) TEM image of PCL nanofibers incubated in 15% PCL-*b*-PEO/ethyl acetate for 60 min.

20 wt % block copolymer solution. At the concentration of 15 wt %, no crystals were observed from the SEM image

after 10 min incubation (Figure 10a). At higher concentrations, crystallites were clearly observed, and the density of

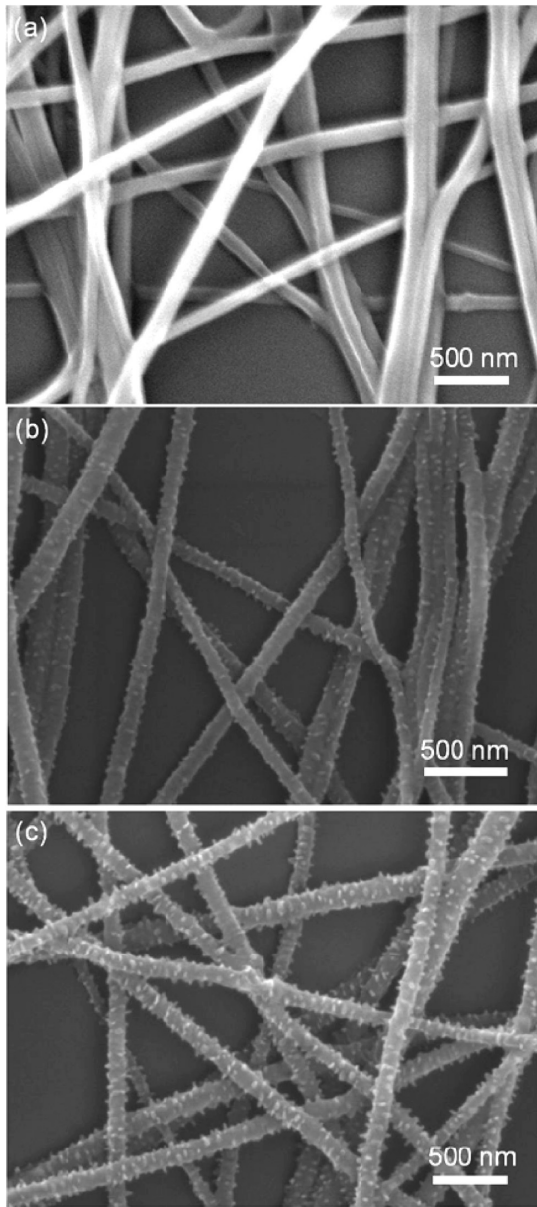


**Figure 10.** PCL nanofibers incubation for 10 min in 15 (a), 18 (b), and 20 wt % (c) PCL-*b*-PEO/ethyl acetate.

nuclei on nanofibers showed an increase from  $2.7 \times 10^{-4}$  nm $^{-2}$  (Figure 10b) to  $3 \times 10^{-4}$  nm $^{-2}$  (Figure 10c). The size of these crystals increased from  $35 \pm 9$  nm (Figure 10b) to  $68 \pm 19$  nm (Figure 10c). In all incubation samples, the thickness of crystals is  $\sim 20$  nm, which is in accordance with the thickness of PCL-*b*-PEO lamellae, and does not vary with incubation condition. Both the size and density of the crystals increase with incubation time and concentration.

The morphology observed in incubation samples (Figures 9 and 10) is quite different from those obtained via solvent evaporation (Figure 6), in which case, because solvent evaporates within several minutes, PCL-*b*-PEO chains phase separate and crystallize along nanofibers, and all the crystals were formed in a relatively short time. Since the crystal growth was fast, a concentration gradient of block copolymer was generated at the crystal growth front, and it varied periodically along the nanofiber axis, leading to the periodical structure of the kebabs as discussed in the CNT-induced polymer crystallization case. However, for the incubation process, as shown in the figures, the kebab crystals were small and the crystallization was slow.

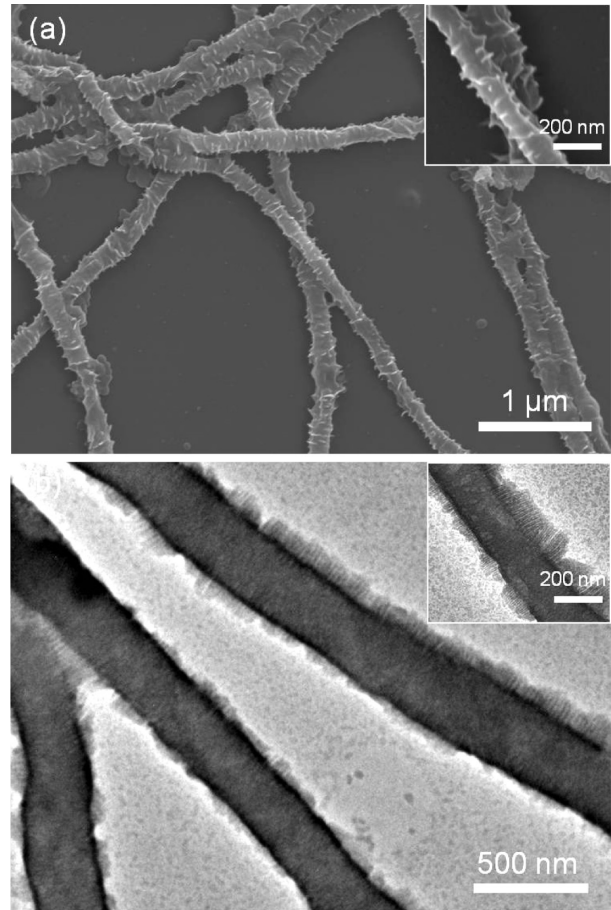


**Figure 11.** SEM (a) and TEM (b) images of PEO nanofibers obtained using solvent evaporation 0.05 wt % PCL-*b*-PEO/DMF.

The slower crystallization process provides more time for a block copolymer chain to diffuse to the growth front; hence, the concentration gradient was largely smeared, which in turn led to the absence of the regular periodic structures of NFSK (Scheme 2).

**PCL-*b*-PEO Crystallization on PEO Nanofibers.** One advantage of NFSK is that the shish and kebab can be formed by different polymers so that the final structure could have different functionality. It would also be of interest to have block copolymer NFSK formed on PEO nanofibers. To this end, PCL-*b*-PEO was dissolved in DMF and deposited on PEO nanofibers via solvent evaporation. It has been demonstrated that DMF itself cannot induce shish-kebab structure on nanofibers.<sup>43</sup> Figure 11 shows SEM and TEM images of PEO nanofibers with block copolymer shish kebab. Different from 2D NFSK<sub>PCL/PCL-*b*-PEO</sub> on PCL nanofibers, block copolymer forms 3D NFSK<sub>PEO/PCL-*b*-PEO</sub> on PEO nanofibers. This is because evaporation of DMF takes much longer time than evaporation of ethyl acetate; therefore, block copolymer was able to concentrate on top of the nanofibers and have enough time to crystallize and form lamellar crystals on the surface of the nanofibers. TEM image of the sample reveals a lamellar structure in block copolymer kebabs. Similar to block copolymer crystallization on PCL nanofibers, the lamellae are relatively perpendicular to PEO fiber axis and the chain folding is parallel to fiber axis.

## Conclusions

Unique hierarchically ordered nanofibers NFSK<sup>PCL/PCL</sup>, NFSK<sup>PCL/PCL-*b*-PEO</sup>, and NFSK<sup>PEO/PCL-*b*-PEO</sup> were obtained by

combining electrospinning and controlled polymer crystallization methods. Electrospun nanofibers served as the shish, and a secondary homopolymer or block copolymer was decorated on the nanofibers in the form of single-crystal lamellae by either an incubation (slow crystallization) or a solvent evaporation (fast crystallization) method. The formation of toroid crystals from crystallites was studied using time-resolved formation of NFSK<sup>PCL/PCL</sup>. Block copolymer with two crystallizable segments, PCL-*b*-PEO in this case, was able to form NFSK structure on both PCL and PEO nanofibers. The formation of shish kebab was attributed to the soft epitaxy mechanism. SAED experiments showed that the polymer chains are parallel with the fiber axis in both the shish and kebab regions. The NFSK structure is of technological interest because it selectively modifies the surface of nanofibers and could introduce multifunctionalities onto the nanofibers in an ordered fashion.

**Acknowledgment.** This work was supported by the National Science Foundation Grants DMR-0804838 and EEC 0649033.

## References and Notes

- (1) Reneker, D. H.; Chun, I. *Nanotechnology* **1996**, 7 (3), 216–223.
- (2) Reneker, D. H.; Yarin, A. L. *Polymer* **2008**, 49 (10), 2387–2425.
- (3) Li, D.; Xia, Y. N. *Adv. Mater.* **2004**, 16 (14), 1151–1170.
- (4) Greiner, A.; Wendorff, J. H. *Angew. Chem., Int. Ed.* **2007**, 46 (30), 5670–5703.
- (5) Burger, C.; Hsiao, B. S.; Chu, B. *Annu. Rev. Mater. Res.* **2006**, 36, 333–368.
- (6) Bazilevsky, A. V.; Yarin, A. L.; Megaridis, C. M. *Langmuir* **2007**, 23 (5), 2311–2314.
- (7) McCann, J. T.; Li, D.; Xia, Y. N. *J. Mater. Chem.* **2005**, 15 (7), 735–738.
- (8) Fong, H.; Chun, I.; Reneker, D. H. *Polymer* **1999**, 40 (16), 4585–4592.
- (9) Ko, F.; Gogotsi, Y.; Ali, A.; Naguib, N.; Ye, H. H.; Yang, G. L.; Li, C.; Willis, P. *Adv. Mater.* **2003**, 15 (14), 1161–1165.
- (10) Yoshimoto, H.; Shin, Y. M.; Terai, H.; Vacanti, J. P. *Biomaterials* **2003**, 24 (12), 2077–2082.
- (11) Chew, S. Y.; Wen, J.; Yim, E. K. F.; Leong, K. W. *Biomacromolecules* **2005**, 6, 2017–2024.
- (12) Pham, Q. P.; Sharma, U.; Mikos, A. G. *Tissue Eng.* **2006**, 12 (5), 1197–1211.
- (13) Liang, D.; Hsiao, B. S.; Chu, B. *Adv. Drug Delivery Rev.* **2007**, 59 (14), 1392–1412.
- (14) Agarwal, S.; Wendorff, J. H.; Greiner, A. *Polymer* **2008**, 49 (26), 5603–5621.
- (15) Dong, B.; Smith, M. E.; Wnek, G. E. *Small* **2009**, 5 (13), 1508–1512.
- (16) Formo, E.; Lee, E.; Campbell, D.; Xia, Y. N. *Nano Lett.* **2008**, 8 (2), 668–672.
- (17) Wang, X. Y.; Drew, C.; Lee, S. H.; Senecal, K. J.; Kumar, J.; Samuelson, L. A. *Nano Lett.* **2002**, 2 (11), 1273–1275.
- (18) Wang, X. Y.; Kim, Y. G.; Drew, C.; Ku, B. C.; Kumar, J.; Samuelson, L. A. *Nano Lett.* **2004**, 4 (2), 331–334.
- (19) Chae, S. K.; Park, H.; Yoon, J.; Lee, C. H.; Ahn, D. J.; Kim, J. M. *Adv. Mater.* **2007**, 19 (4), 521–524.
- (20) Lin, T.; Wang, H.; Wang, X. *Adv. Mater.* **2005**, 17 (22), 2699–2703.
- (21) Li, D.; Xia, Y. N. *Nano Lett.* **2004**, 4 (5), 933–938.
- (22) Roh, K.-H.; Martin, D. C.; Lahann, J. *Nature Mater.* **2005**, 4 (10), 759–763.
- (23) Sanders, E. H.; Kloefkorn, R.; Bowlin, G. L.; Simpson, D. G.; Wnek, G. E. *Macromolecules* **2003**, 36 (11), 3803–3805.
- (24) Sun, Z. C.; Zussman, E.; Yarin, A. L.; Wendorff, J. H.; Greiner, A. *Adv. Mater.* **2003**, 15 (22), 1929–1932.
- (25) Zhang, Y. Z.; Huang, Z. M.; Xu, X. J.; Lim, C. T.; Ramakrishna, S. *Chem. Mater.* **2004**, 16 (18), 3406–3409.
- (26) Loscertales, I. G.; Barrero, A.; Márquez, M.; Spretz, R.; Velarde-Ortiz, R.; Larsen, G. *J. Am. Chem. Soc.* **2004**, 126 (17), 5376–5377.
- (27) Li, D.; Wang, Y. L.; Xia, Y. N. *Adv. Mater.* **2004**, 16 (4), 361–366.
- (28) Jiang, L.; Zhao, Y.; Zhai, J. *Angew. Chem., Int. Ed.* **2004**, 43 (33), 4338–4341.
- (29) Acatay, K.; Simsek, E.; Ow-Yang, C.; Menceloglu, Y. Z. *Angew. Chem., Int. Ed.* **2004**, 43 (39), 5210–5213.
- (30) Deitzel, J. M.; Kosik, W.; McKnight, S. H.; Tan, N. C. B.; DeSimone, J. M.; Crette, S. *Polymer* **2002**, 43 (3), 1025–1029.
- (31) Megelski, S.; Stephens, J. S.; Chase, D. B.; Rabolt, J. F. *Macromolecules* **2002**, 35 (22), 8456–8466.
- (32) Bognitzki, M.; Czado, W.; Frese, T.; Schaper, A.; Hellwig, M.; Steinhart, M.; Greiner, A.; Wendorff, J. H. *Adv. Mater.* **2001**, 13 (1), 70–72.
- (33) Ruotsalainen, T.; Turku, J.; Heikkilä, P.; Ruokolainen, J.; Nykänen, A.; Laitinen, T.; Torkkeli, M.; Serimaa, R.; ten Brinke, G.; Harlin, A.; Ikkala, O. *Adv. Mater.* **2005**, 17 (8), 1048–1052.
- (34) Babel, A.; Li, D.; Xia, Y.; Jenekhe, S. A. *Macromolecules* **2005**, 38 (11), 4705–4711.
- (35) Theron, A.; Zussman, E.; Yarin, A. L. *Nanotechnology* **2001**, 12 (3), 384–390.
- (36) Dersch, R.; Liu, T. Q.; Schaper, A. K.; Greiner, A.; Wendorff, J. H. *J. Polym. Sci., Part A: Polym. Chem.* **2003**, 41 (4), 545–553.
- (37) Kameoka, J.; Craighead, H. G. *Appl. Phys. Lett.* **2003**, 83 (2), 371–373.
- (38) Li, D.; Wang, Y. L.; Xia, Y. N. *Nano Lett.* **2003**, 3 (8), 1167–1171.
- (39) Kalra, V.; Mendez, S.; Lee, J. H.; Nguyen, H.; Marquez, M.; Joo, Y. L. *Adv. Mater.* **2006**, 18 (24), 3299–3303.
- (40) Ma, M. L.; Krikorian, V.; Yu, J. H.; Thomas, E. L.; Rutledge, G. C. *Nano Lett.* **2006**, 6 (12), 2969–2972.
- (41) Fong, H.; Reneker, D. H. *J. Polym. Sci., Part B: Polym. Phys.* **1999**, 37 (24), 3488–3493.
- (42) Ji, L. W.; Zhang, X. W. *Nanotechnology* **2009**, 20 (15), 155705–155712.
- (43) Wang, B.; Li, B.; Xiong, J.; Li, C. Y. *Macromolecules* **2008**, 41 (24), 9516–9521.
- (44) Geil, P. H. *Polymer Single Crystals*; Robert E. Krieger Pub: Juntington, 1973.
- (45) Yoshioka, T.; Dersch, R.; Tsuji, M.; Schaper, A. K. *Polymer* **2010**, 51 (11), 2383–2389.
- (46) Li, C. Y. *J. Polym. Sci., Part B: Polym. Phys.* **2009**, 47 (24), 2436–2440.
- (47) Li, C. Y.; Li, L.; Cai, W.; Kodjie, S. L.; Tenneti, K. K. *Adv. Mater.* **2005**, 17 (9), 1198–1202.
- (48) Li, L.; Li, C. Y.; Ni, C. *J. Am. Chem. Soc.* **2006**, 128 (5), 1692–1699.
- (49) Li, L.; Yang, Y.; Yang, G.; Chen, X.; Hsiao, B. S.; Chu, B.; Spanier, J. E.; Li, C. Y. *Nano Lett.* **2006**, 6 (5), 1007–1012.
- (50) Li, L.; Li, B.; Yang, G.; Li, C. Y. *Langmuir* **2007**, 23 (16), 8522–8525.
- (51) Li, L.; Li, C. Y.; Ni, C.; Rong, L.; Hsiao, B. *Polymer* **2007**, 48 (12), 3452–3460.
- (52) Li, L.; Li, B.; Hood, M. A.; Li, C. Y. *Polymer* **2009**, 50 (4), 953–965.
- (53) Kim, H. C.; Rettner, C. T.; Sundstrom, L. *Nanotechnology* **2008**, 19 (23), 235301–235305.
- (54) Li, B.; Li, L.; Wang, B.; Li, C. Y. *Nature Nanotechnol.* **2009**, 4 (6), 358–362.